A Conceptual Framework for Integrating Blue Carbon Ecosystems into Climate Mitigation and Coastal Flood Risk Reduction for Power Plants

Intan Pamungkas[1*, a)], Yoga Edi Kuncaraningrat[2, b)], Meiri Triani [1, c)]

[1] *Puslitbang (Research Institute), PT PLN (Persero), Jakarta, Indonesia*
[2]*Soil Geography and Landscape Group, Wageningen University & Research, Wageningen, the Netherlands*

*[a)]intan.pamungkas@pln.co.id
[b)]kuncaraningratediyoga@gmail.com
[c)]meiri.triani@pln.co.id

Abstract. Coastal coal-fired power plants (CFPPs) in Indonesia are increasingly facing risks from sea-level rise (SLR) and flooding. In line with Indonesia's 2030 NDC and carbon valuation rules, this study creates a framework that connects mangrove suitability, carbon storage, and flood-risk assessment. This aims to support climate-resilient planning for energy infrastructure. The framework is applied to the Suralaya CFPP under four scenarios: Baseline 2025, Mangrove 2025, SLR 2030, and SLR + Mangroves 2030. Results show that the limited suitable area of 145.23 ha results in a modest carbon storage of 927 tons of CO2 annually, which equals 27.81 million IDR in avoided carbon costs. Mangrove restoration reduces the flooded area by approximately 11% (≈60 ha) under baseline 2025 conditions and by about 22% (≈125 ha) under SLR 2030 scenario. The restoration reduced flood risk from Significant to Moderate under baseline 2025 conditions. However, it couldn't reduce the risk level in the SLR 2030 scenario. These findings demonstrate that while mangroves provide measurable co-benefits for carbon storage and flood attenuation, they are insufficient as a standalone solution. Additional emissions-mitigation technologies such as carbon capture and storage (CCS), as well as engineered flood-protection measures may be needed to manage residual climate risk. The proposed framework functions as a decision-support tool for government and industry by revealing the physical limits of nature-based solutions and identifying where complementary interventions are required. Overall, the framework offers a transferable approach for integrating blue-carbon ecosystems into climate-risk assessments and sustainable energy-transition strategies for Indonesia's coastal power sector.

Keywords: blue carbon, carbon sequestration, coastal resilience, flood risk reduction, mangrove restoration

1 Introduction

Climate risk is projected to remain the most significant global threat in the next decades, highlighting the urgent need for integrated mitigation and adaptation strategies. Numerous studies indicate that the impacts of climate change have affected multiple sectors, including the power sector, resulting in financial losses, environmental degradation, and threats to human life. Carbon emission reduction within the power sector is widely acknowledged as a critical global climate change mitigation strategy, given the sector's substantial contribution to total carbon emissions. This contribution is largely driven by the continued dependence on coal as the dominant energy source, particularly in many emerging economies [39].

Indonesia's coal-fired power plants (CFPPs) are predominantly located in coastal zones and remain essential to meeting the country's baseload electricity demand, supporting both industrial activity and national energy security. PT. PLN, Indonesia's state-owned electricity utility, operates 135 CFPPs with a total installed capacity of approximately 20.44 GW, making coal the backbone of national electricity generation [9]. Most CFPPs are located in coastal areas to facilitate access to seawater for cooling and coal transportation. However, facilities situated on low-lying shorelines are particularly vulnerable to climate-related hazards. Rising sea levels, intensifying storm surges, and recurrent tidal flooding threaten the continuity of these operations, leading to significant disruptions, economic

L. R. Sugiarti et al. (eds.), *Proceedings of the 2nd International Conference on Social Environment Diversity (ICOSEND 2025)*, Advances in Social Science, Education and Humanities Research 1011,
https://doi.org/10.2991/978-2-38476-565-2_7

losses, and heightened safety concerns. Despite these mounting risks, coastal CFPPs are projected to remain a vital component of Indonesia's power system in the near term [42]. Consequently, the increasing physical vulnerability of coastal CFPPs presents significant challenges to both infrastructure resilience and long-term energy security.

At the same time, CFPPs are among the largest contributors to Indonesia's greenhouse gas emissions. As Indonesia pursues its net-zero emissions target by 2060 and its interim commitments under the 2030 Nationally Determined Contribution (NDC) to the Paris Agreement, there is increasing pressure to reduce carbon intensity while maintaining power-system reliability. These commitments are reinforced by the Government of Indonesia policies such as Presidential Regulation No. 98 of 2021 on Carbon Economic Value (Nilai Ekonomi Karbon, NEK), and the recent Minister of Marine Affairs and Fisheries Regulation No. 1 of 2025, which extends NEK implementation to the marine sector, including blue-carbon ecosystems.

Current mitigation planning prioritizes technological approaches such as Carbon Capture and Storage (CCS), which separates, treats, compresses, and transports carbon dioxide to secure geological reservoirs [34].

CCS can substantially reduce stack emissions from existing coal-fired power plants and is therefore positioned as a central component of the national climate mitigation pathway. However, it addresses only one dimension of the broader challenge. CCS does not reduce the growing physical coastal risks faced by power infrastructure and provides limited ecological co-benefits. On its own, CCS remains insufficient to safeguard long-term operational reliability or to support broader environmental resilience.

Natural ecosystems provide a complementary pathway for strengthening coastal resilience while functioning as significant carbon sinks [2]. These dual roles underpin the broader concept of nature-based solutions, which seek to reduce climate impacts and enhance the adaptive capacity of ecosystems and communities. Among the various approaches, blue carbon ecosystems represent one of the most promising strategies for simultaneously advancing mitigation and adaptation objectives. Mangroves, seagrasses, and salt marshes sequester carbon at rates exceeding most terrestrial forests, while also mitigating tidal flooding and sea-level-rise-amplified coastal hazards through wave attenuation, sediment stabilization, and storm surge buffering. They further support biodiversity and sustain coastal livelihoods [11]. Although each blue carbon ecosystem plays an important role, their relevance varies by geomorphology and ecosystem distribution. In the Indonesian coastal context, mangroves are the dominant and most spatially extensive blue carbon system, occurring primarily in estuarine and low-lying coastal zones [35] where many coal-fired power plants are situated. As a result, mangroves represent the most applicable blue carbon ecosystem strategies that seek to integrate climate mitigation and coastal risk reduction for industrial infrastructure.

Mangrove-based carbon sequestration creates tangible economic value through its function as a regulating ecosystem service. This value is coherent within Indonesia's carbon policy framework, particularly through the implementation under Presidential Regulation 98 of 2021. Indonesia's carbon pricing architecture, comprising the national carbon tax mandated by the Harmonized Tax Law, emerging emission trading arrangements initiated through the power sector cap and trade pilot, and the voluntary carbon market regulated under the Ministry of Environment and Forestry, provides formal mechanisms for converting sequestered carbon into tradable credits or compliance units. Aligning estimated sequestration rates with these pricing instruments enable mangrove restoration to contribute not only to emission reduction targets but also to the generation of carbon credits that can support national decarbonization pathways. This positioning frames mangrove ecosystems as both a mitigation asset and an economically quantifiable nature-based solution that complements technology-driven measures such as CCS.

Indonesia holds an especially strategic position in this regard, containing approximately twenty-four percent of the world's mangroves [4]. Mangrove forests are critical not only because of their extensive spatial coverage but also because of their exceptional capacity for long-term carbon sequestration and their effectiveness in attenuating coastal flooding [11]. Despite increasing recognition of blue carbon's role in global climate mitigation, its potential contribution to risk management for coastal CFPPs remains underexplored. Most studies on blue carbon focus on sequestration potential or ecosystem restoration, with limited attention to its integration into industrial and infrastructure resilience planning.

The novelty of this study lies in integrating ecological suitability, blue carbon valuation, and flood-risk assessment within a single conceptual framework tailored to coastal power plant infrastructure. This paper proposes a conceptual framework to evaluate the dual role of blue carbon ecosystems in enhancing resilience to protect CFPPs from climate disaster risks and supporting low-carbon development in coastal energy infrastructure. By linking climate mitigation and risk reduction, this study contributes to the growing discourse on sustainable energy transition and coastal adaptation strategies in strengthening climate resilience capacity in Indonesia.

2 Method

2.1 Literature-Guided Framework Development

The methodological design of this study is grounded in a structured synthesis of multiple strands of literature relevant to ecosystem-based climate mitigation and adaptation in coastal energy systems. Rather than treating these domains in isolation, the approach integrates insights from (i) land-suitability analysis and carbon sequestration [1], and economic valuation of carbon credits [11]; and (ii) coastal flood simulation [18], climate-risk assessment [41], and quantification of mangrove-based risk-reduction effects [51]. This synthesis identifies key conceptual intersections that support the development of a unified framework for assessing the role of mangrove restoration in enhancing the resilience of coastal coal-fired power plants (CFPPs).

Literature on mangrove ecology and restoration suitability provides the biophysical basis for identifying areas capable of sustaining mangrove establishment and long-term carbon storage [1]. This body of work informs the selection of spatial, geomorphological, soil, and climatological parameters used to conceptualize mangrove land suitability and carbon-sequestration potential, including the influence of elevation, sediment dynamics, climate and hydrological gradients. Together, these parameters define an ecologically coherent spatial boundary for subsequent analysis [32, 42, 54]. In parallel, economic valuation literature and Indonesia's evolving carbon-pricing and incentive mechanisms establish the basis for translating biophysical carbon sequestration into monetary value [11]. This ensures that land suitability, sequestration potential, and economic valuation are assessed within a consistent analytical context.

Complementary literature on coastal hydrodynamics, flood modelling, and climate-risk assessment clarifies how tidal inundation processes and infrastructure sensitivity interact to shape coastal vulnerability [3, 19, 41, 52]. These studies demonstrate the mechanisms through which mangrove vegetation alters coastal flood dynamics by modifying surface resistance, attenuating flow velocity, influencing sediment transport, and reducing flood intensity [16, 30, 51]. Insights from this literature inform the representation of flood progression and risk-reduction functions within the framework.

Building on this literature synthesis, a conceptual framework was developed through a sequential and integrative process that identifies key processes linking mangrove restoration to both carbon sequestration and tidal flood mitigation. These processes were translated into explicit conceptual linkages describing how future mangrove suitability informs carbon benefits, how restored mangroves alter tidal flood dynamics, and how resulting mitigation outcomes can be evaluated in economic terms under Indonesia's carbon-pricing mechanisms [1, 11]. The resulting unified modelling structure provides a coherent basis for assessing the role of blue-carbon ecosystems in supporting low-emission, climate-resilient coastal energy systems, particularly in relation to mitigation and adaptation strategies for coastal CFPPs.

2.2 Analytical System Boundaries and Study Area

The framework is designed for a representative CFPP located in low-lying coastal terrain, where mangrove restoration and tidal inundation dynamics interact directly with infrastructure exposure. The observation or analytical boundary is defined to encompass ecological processes relevant to mangrove establishment, hydrodynamic processes governing tidal flooding, and the sensitivity profile of coastal energy assets.

The study area is defined as a 20 × 20 km spatial extent centered on PT PLN's Suralaya CFPP, Pulomerak Municipality, Cilegon City, Banten Province, Indonesia and is adopted as the spatial boundary of the analysis. The study area covers coastal zones of most Cilegon District, bounded by 5.0°S–7.0°S and 105.0°E–107.0°E. PT. PLN's Suralaya CFFP can be reached with a 1-hour car drive from Cilegon city. Based on the Indonesian National Digital Elevation Model (DEMNAS), the highest elevation within the study area reaches 582.5 m above mean sea level [7], while bathymetric data from the General Bathymetric Chart of the Oceans (GEBCO) indicate a minimum elevation of −106 m below mean sea level (Tozer et al., 2019).

The ten-kilometer radius of the analysis domain, which includes offshore and nearshore marine areas, is consistent with previous work on mangrove suitability mapping and coastal flood analysis by Syahid et al. (2020). The importance of including sea area is further supported by [51], who demonstrate that even relatively small landward displacements of mangrove forests (≈100 m) can increase human flood risk by approximately 17%. This highlights the critical role of near-coastal mangrove dynamics in shaping flood-risk outcomes and underscores the need to explicitly incorporate marine and coastal transition zones within the analytical domain. Accordingly, subsequent analyses explicitly include sea areas to ensure a realistic representation of hydrodynamic processes and mangrove–flood interactions.

Tide-driven coastal flooding and Sea Level Rise for future scenarios are selected as the primary climate hazard due to its strong relevance for coastal infrastructure and its direct sensitivity to mangrove-mediated hydrodynamic

processes. Accordingly, the analytical boundary integrates land-suitability assessment, carbon-sequestration modelling with economic valuation, and rule-based tidal flood-progression simulation within a climate-risk assessment framework aligned with the climate risk from IPCC Sixth Assessment Report and ISO 14091:2021 procedure [27].

2.3 Application of the Framework to a Coastal CFPP in Indonesia

The proposed conceptual framework is applied to a coastal coal-fired power plant (CFPP) in Banten Province, Indonesia, with an installed capacity of 4,025 MW. The facility is representative of large baseload power stations located on low-elevation coastal terrain and exposed to tidal inundation. Its geomorphological setting and hazard profile align with the defined system boundaries, making it suitable for evaluating coastal climate-risk dynamics.

This case study operationalizes all analytical components of the framework, including land-suitability analysis, carbon-sequestration estimation, rule-based tidal flood-progression simulation, and climate-risk assessment within a realistic spatial and hydrodynamic context. Rather than serving as full empirical validation, the case functions as an engineering-oriented demonstration of how the integrated framework can be applied to assess mitigation potential and flood-attenuation performance of mangrove-based interventions for coastal energy infrastructure.

3 Result

3.1 Carbon Sequestration

Data collection and evaluation. Data used in this study are grouped into two main categories: (i) static spatial data and (ii) hydrological and climate time-series data. Static spatial datasets were used to represent physical and land-surface characteristics of the study area. These include topography, bathymetry, land cover, LAI, soil textures, and infrastructure datasets. Elevation data were obtained from the Indonesian Geospatial Agency (Badan Informasi Geospasial or BIG), providing the National Digital Elevation Model (DEMNAS), while bathymetric information was derived from the General Bathymetric Chart of the Oceans (GEBCO). Land use and land cover data were sourced from ESA WorldCover and BIG. The main CFFB infrastructure and PLN facility area was created by digitizing areal picture/imagery.

Hydrological and climate variables were collected as time-series data with hourly, daily, monthly, and annual temporal resolutions, depending on their availability and variable. These data include precipitation, air temperature, tide water levels, and storm surge obtained from Earth Data Nasa CMIP6 climate projections, and Climate Hazards Center (CHC), which are relevant to mangrove suitability and will be put as forcings in the coastal flooding model. Time-series data span the period 2019–2030, covering 11 years to capture both historical conditions and future projection scenarios of mangrove suitability and flood risk benefits.

Bulk downloading of large climate and hydrological datasets such as .tifs and netcdf was conducted using Python-based workflows and command-line tools via Cygwin. This approach enabled automated retrieval of multi-year, high-temporal-resolution (daily to hourly) data from remote servers, ensuring consistency and efficiency in data acquisition. Downloaded .tif datasets were organized and checked using ArcGIS Pro for their coverage.

Precipitation data were evaluated by comparing them with observations from the Indonesian Agency for Meteorology, Climatology, and Geophysics (BMKG) using R-studio. Satellite-based CHIRPS precipitation data were downloaded from the Climate Hazards Center (CHC), University of California, and spatially clipped using Python to the study domain bounded by 5.0°S–7.0°S and 105.0°E–107.0°E. Daily CHIRPS data were evaluated against BMKG observations only for the available historical period 2019–2024. BMKG precipitation data were obtained from the station nearest to the Suralaya coal-fired power plant (CFPP), located in Serang City at approximately 41.5 km south of the CFPP. The comparison between daily BMKG observations and CHIRPS precipitation indicates low agreement at the daily scale, with a negative NSE (−0.27) and a low KGE (0.01). Error metrics indicate minimal systematic bias (ME = 0.25 mm), but substantial random error (RMSE = 13.32 mm), associated with high-intensity rainfall events.

Areas unsuitable for mangrove restoration were identified based on existing land uses that constrain ecological recovery. Land use and land cover data from ESA WorldCover were used to delineate built-up and agricultural classes. LAI was used to also confirm areas that are already densely vegetated by forests. These were cross validated with building polygons from OpenStreetMap (OSM) and Badan Informasi Geospasial (BIG) to identify areas already occupied by settlements, industrial facilities, and transportation networks. Overlapping results across datasets were interpreted as permanent land-use constraints where mangrove restoration is not feasible. This process was done using

ArcGIS Pro.

To examine differences between current (2019–2024) and future (2025–2030) climate conditions or periods, descriptive statistics were conducted for precipitation, air temperature, and tidal water levels within each period. Time-series data were grouped using within-period quantiles to identify shifts in climatic dominance and potential abrupt changes relevant to mangrove suitability and coastal flooding. Air temperature shows limited variability across 2019 to 2030. Monthly mean air temperatures range from a minimum of 26.6 °C in 2021 to a maximum of 28.34 °C in 2023, with both the 2019–2024 and 2025–2030 periods consistently averaging around 26–27 °C, which is classified as suitable based on Table 2.

Precipitation exhibits stronger interannual variability. When aggregated into dominant regimes, high-precipitation years occur mainly during 2019–2024, with annual averages ranging from 1,167 to 2,174 mm, while lower-precipitation years dominate 2025–2030, with annual averages between 1,251 and 1,819 mm. All values fall within a very suitable range for mangrove growth.

Tidal water levels show a clear increase in the future period, consistent with sea-level rise. Mean tidal levels during 2025–2030 are approximately 144% of those observed in 2019–2024. Low-tide years (2019–2024) range from 2.3 to 10.7 cm, whereas high-tide years (2025–2030) range from 6.01 to 14.4 cm, indicating increased inundation frequency and depth. Tidal 2019 to 2030 is classified as very suitable based on Table 2 (Primavera et al., 2012). Tide, precipitation, and air temperature .tif files were all averaged through python script within current (2019-2024) and future (2025-2030) climate periods to be used for land suitability analysis.

Overall, precipitation and tidal inundation are classified as very suitable in all areas, and air temperature is suitable in all areas. Following the limiting-factor principle, overall climate suitability for mangrove establishment is therefore classified as suitable, following air temperature as the lower suitability determinant and only differentiated by sea level rise of 144% 2025-2030 compared to 2019-2024. All statistical, climate suitability, and quantile value analysis within the periods were done using R-Studio.

Spatial land suitability analysis. The spatial land suitability analysis identifies areas with potential for mangrove restoration by integrating multiple biophysical parameters: climate (air temperature and precipitation), geomorphology (elevation and slope), soil texture, and coastal hydrodynamics (tidal inundation and bathymetry). All spatial data layers are standardized to a uniform coordinate system (WGS 1984 UTM Zone 48S) and resolution to ensure consistency in spatial extent. Each parameter input data for the suitability map is reclassified according to the mangrove suitability threshold value range derived from previous studies (Table 1), following the multi-criteria classification using conditional statements "if x is between, or less or more than" in R-studio described by [47]. Spatial mangrove land-suitability analysis was conducted using raster-based workflows in R-studio, primarily applying the terra, sf, and stars packages.

For elevation land suitability analysis, DEMNAS (elevation raster data) were first clipped to a coastline-focused shapefile that delineates coastline and the CFPP facility areas such as harbours, storage yards, cranes, and other operational infrastructure. This shapefile was buffered by 20 m and used to spatially mask and crop the DEMNAS raster. Bathymetric data were resampled to 8 m resolution to match DEMNAS using bilinear interpolation in ArcGIS Pro and mosaicked with the clipped DEMNAS to generate a continuous elevation surface representing both above- and below-sea-level terrain within the 20 × 20 km spatial extent centered on the main CFPP. The buffer, clip, and overwriting using mozaic to raster geoprocessing was done in ArcGIS Pro. Mangrove elevation suitability was reclassified following thresholds proposed by [32] resulting in predominantly very suitable (S3) coastal and near-shore raster cells and offshore grid blocks derived from the original 50 m bathymetry resolution, with limited suitable (S2) and moderately suitable (S1) areas occurring in isolated onshore raster cells.

Mangrove slope suitability was derived from elevation (DEMNAS mosaiced with GEBCO bathymetry) that was geoprocessed with slope tool in ArcGIS Pro, then reclassified into suitability classes following Syahid et al., 2020. For mangrove soil-texture suitability, soil sand, silt, and clay percentage spatial spread data from SoilGrids of soil depths 0-80 cm are averaged. Then, averaged data are classified following [42] mangrove sand, silt, and clay suitability. Suitability classified sand, silt, and clay layers were stacked and combined using a minimum-rule overlay. Final single land suitability map took the lowest score among elevation, slope, and soil suitability maps. Because soil data are unavailable offshore and in coastline, offshore and coastline were assumed clay-dominated and evaluated using elevation and slope raster data only. This resulted in 117 ha classified as very suitable (S3) along the coast and offshore. While inland areas with soil data yielded 22.58 ha of suitable (S2) and 5.56 ha of moderately suitable (S1) land. In total, 145.23 ha was identified as having suitability scores greater than unsuitable (S0) for mangrove restoration. This process resulted in the Mangrove Land Suitability Map.

Carbon sequestration and economic valuation. According to [1], mangrove forests sequester carbon at an average rate of 6.38 tons of carbon per hectare per year (tonC ha year-1). The potential carbon sequestration for future mangrove restoration is estimated using the following simplified formula:

$$C = A \times R \quad (1)$$

Where C is the annual sequestration potential (tons of CO_2 year-1), A is the area suitable for mangrove restoration (ha), and R is the average sequestration rate per hectare per year (tons CO_2 ha-2 year-1). For the 145.23 hectares identified as suitable for restoration, applying an average sequestration rate of 6.38 tons of CO_2 per hectare per year yields an estimated annual uptake of approximately 927 tons of CO_2. Relative to the CFPP's estimated annual emissions of 24 million tons CO_2, this contribution represents approximately 0.004%.

The economic valuation is derived using Indonesia's regulated carbon price of Rp 30,000 per ton CO_2, under Law No.7 of 2021 on Harmonization of Tax Regulations. Based on this pricing level, the estimated sequestration corresponds to an avoided carbon cost of approximately Rp 27.81 million per year. Although modest compared to total emissions, this valuation highlights the economic relevance of mangrove conservation as a nature-based mitigation instrument within Indonesia's carbon pricing architecture.

3.2 Flood Simulation

The topographic input as a basis of simulating water movement in NetLogo flood simulation which is called as the Baseline 2019-2025 (current/baseline) DEM, was done in ArcGIS Pro by doing mozaic to raster to implement the coastline-clipped DEMNAS on top of a uniformly one-meter desk elevation representing a uniform sea water level throughout the 20 × 20 km study area spatial extent. Most negative elevations in the coastline of the DEMNAS are turned into a value of 1 m.

The flood model was developed in NetLogo using a cellular automata (CA) structure in which each cell represents a terrain cell with attributes such as elevation, water depth, hydraulic head, water storage capacity, and flooding status. This modeling approach is intended to enable relative, scenario-based comparisons of flood behavior rather than predictive accurate hydrodynamic simulation. The input data consists of ASCII raster files modified from the Baseline 2019-2025 DEM. The Baseline 2019-2025 DEM has been resampled from an eight-meter to a sixty-meter cell size resolution to reduce computational time. Tif to ASCII and resampling was done using ArcGIS Pro. During initialization, each cell receives its elevation, "dry" cell status, and an initial water storage capacity based on the elevation difference between the center cell and its neighboring cells. Flooding is initiated at eleven designated influx points evenly distributed along the study area coastlines, with each influx point delivering water at a rate of 10 m3 per second. This flow rate was determined through trials using different influx rates to find the one that best represents the speed of Suralaya tidal water based on [19].

A basic flux–velocity ($v = Q/A$) shows that 10 m³ per second (applied in the model) across a 60 m wide grid cell with ~1 m effective depth implies $v \approx 0.17$ m per second, which is comparable in magnitude to a reported Suralaya coastal current speed of 0.12 m per second [19], supporting the physical plausibility of the chosen inflow rate. The inflows from each influx point are sequentially redistributed to neighboring cells based on a multiple flow algorithm, which will distribute the amount of water from the center cell to its neighbor evenly based on the fraction of elevation difference between the center cell and its eight neighboring cells.

Water movement follows a multiple-flow algorithm, conceptually aligned in which water flows from one cell to its multiple neighbors based on differences in total head (elevation + water depth). At each tick that represents one minute. Cells with water compare their water total heads with those of surrounding cells and transfer water horizontally, thereby reducing their head differences. When a cell receives water, it receives flooded status and turns blue. Water spread in a circular motion from each of the eleven influx points. After the coastlines of Suralaya have been filled with water and it cannot breach further into the land, the water starts filling the cell behind them with a lower water total head, away from the coastlines. Until the water fills up the outer study area boundary, it starts to fill up again towards the coastlines and repeats the same pattern, creating oscillating motion similar to cycles of low tides and high tides.

Representation of Mangroves and Sea Level. Mangroves characteristics, including the presence or absence of mangroves, and spaces between them were represented indirectly through the elevation raster rather than by modifying hydrodynamic coefficients within the model or adding a manning's number layer. Each scenario raster was converted into an ASCII grid in which mangrove-covered areas are defined by an additional two-meters of elevation. Because the model derives each patch's water-storage capacity, hydraulic head, and flow behavior directly from elevation,

these DEM (thus ASCII) elevation differences allow mangrove vegetation to influence flood behavior without requiring additional code-based parameters. Mangrove zones were assigned modified surface values that simulate their natural ability to retain water, reduce flow velocity, and buffer inland areas against flooding.

The mangrove presence was represented by a two-meter increase in elevation in the 60-meter cell size DEM. This two-meter elevation increase was assigned to specific areas by distributing random points using *Create Random Points* geoprocessing tool within a previously defined suitability area, done in ArcGIS Pro. For areas classified as "very suitable" (S3), two thousand random points were distributed across approximately 117 hectares, maintaining a minimum distance of five meters between each point. In contrast, for "suitable" (S2) and "moderately suitable" (S1) areas, fifty random points were placed within a total of 28.23 hectares, keeping a minimum distance of ten meters between them. These points were assigned a value of "1" (meter) and geoprocessed using the *point-to-raster* tool with a cell size of sixty meters in ArcGIS Pro. Then, *raster calculator* was employed to multiply the new mangrove raster by two, creating cells with elevation of two meters. Finally, the resulting two-meter elevation mangrove Digital Elevation Model (DEM) cells were integrated with the baseline DEM and the sea-level rise scenario DEM to incorporate the effects of mangroves. Each simulation scenario is represented by a separate elevation raster, then used as NetLogo input.

TABLE 1. Biophysical parameters for land suitability

Parameter	Class	Class Value	Reference
Air temperature (°C)	Very suitable	28-30	(Monsef et al., 2013; Syahid et al., 2020)
	Suitable	26-28 & 30-32	
	Moderate	8-26 & 32-42	
	Unsuitable	<8 & >42	
Precipitation (mm)	Very suitable	1400-3750	(Duke, 1992; Syahid et al., 2020)
	Suitable	1200-1400; 3750-4500	
	Moderate	0-1200; 4500-7500	
	Unsuitable	>7500	
Elevation (m)	Very suitable	(-0.2) - 1.6	(Leong et al., 2018)
	Suitable	(-0.10) - (-0.2); 1.6 - 2.2	
	Moderate	(-2.0) - (-1.0); 2.2 - 2.8	
	Unsuitable	<-2.0 or >2.8	
Slope (%)	Very suitable	0-1	(Suprakto & Arfiati, 2014; Syahid et al., 2020)
	Suitable	2-2.15	
	Moderate	2.15-2.5	
	Unsuitable	>2,5	
Tides (m)	Very suitable	≤0.4	(Clarke & Hannon, 1969; Primavera et al., 2012)
	Suitable	0.4-0.3	
	Moderate	0.3-1.27	
	Unsuitable	>1.27	

TABLE 2. Mangrove soil texture suitability table based on Saputriningrum & Mardiatno, 2018.

Suitability score	Suitability class	Sand (%)	Silt (%)	Clay (%)	Representative USDA texture(s)
3	Very suitable	< 25	25–45	> 35	Clay, Silty Clay

2	Suitable	< 35	30–60	25–40	Silty Clay Loam, Clay Loam
1	Moderate	35–65	10–40	15–30	Sandy Clay Loam, Sandy Clay
0	Unsuitable	<35 & >65	<10 & >40	<15 & >30	Other textures

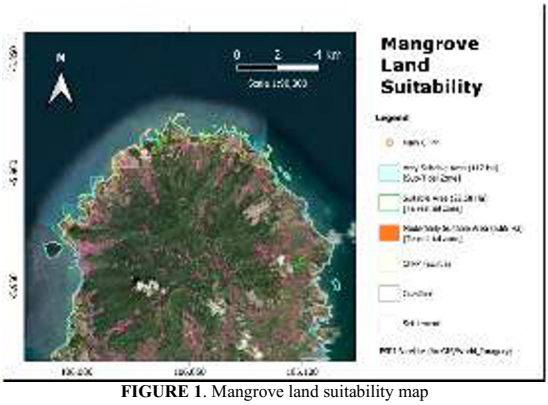

FIGURE 1. Mangrove land suitability map

The sea level rise scenario is developed by comparing the average sea level from 2019 to 2024 (current) with the average sea level from 2025 to 2030 (future) using tide data from the same database. This classification into the two periods (2019-2024 and 2025-2030) was performed in R-studio by calculating the average annual values. The average tide water level from 2025 to 2030 is found generally to be 144% of the tide level recorded from 2019 to 2024. Consequently, the previous uniform elevation raster was adjusted to represent a height of 1.443 meters to create the 2025 to 2030 scenario.

To make the 2025 to 2030 scenario DEMs, this raster was combined with the coastline-clipped Digital Elevation Model (DEMNas). The most negative elevations around the DEMNas coastline were converted to 1.443 meters, following the baseline process for creating the DEM for 2025. Each Digital Elevation Model (DEM), representing a distinct scenario, was input into NetLogo and simulated separately in an individual model run. For each scenario, the model was executed with a constant water influx of 10 m^3/s over a six-day (158-hour) simulation period or model time. This duration was selected to approximate the maximum potential coastal flooding event in West Java under extreme conditions.

Scenario Design. Four simulation scenarios were developed to evaluate the combined and isolated effects of mangrove presence and sea-level rise. The scenarios being used in these simulations are:

1. Baseline 2025 (Without Mangroves): Represents current land-cover conditions in 2025 without mangrove vegetation. The DEM reflects existing topography with no additional micro-topographic adjustments.
2. Mangrove 2025 (Baseline with Mangroves): Uses the 2025 DEM but incorporates restored mangrove areas through adjusted elevation values. These modifications increase water retention capacity in mangrove areas, reduce overland flow speeds, and are expected to capture the protective effect of mangroves under present- day sea levels.
3. Sea Level Rise 2030 (Without Mangroves): Represents projected 2030 sea levels under climate change by elevating the uniform 20 x 20 km desk elevation representing a uniform sea water level from 1 meter to
4. 1.44 meter. No mangroves are included. This scenario evaluates how higher sea levels alone influence breach behavior, inland flood propagation, and exposure in low-lying areas.
5. Sea Level Rise + Mangroves 2030: Combines projected 2030 sea-level rise with mangrove presence. Mangrove areas are again represented through an additional two-meter elevation with the same configuration as the Mangrove 2025 scenario, but within a raster where the sea level is higher. This scenario allows assessment of whether mangroves can mitigate increased flood risks associated with rising sea levels.

Each raster scenario went through six hours (model time) of coastal flooding, allowing for a direct comparison of

how mangroves and rising sea levels influence flood extent, depth, and spatial distribution. The outcomes of each scenario are illustrated in Figures 3 and 4, while the progression of flood area throughout 80 hours can be observed in Figures 5 and 6.

Flooded area progression was quantified using time-step flood area maps output from the NetLogo cellular flood model, exported as ASCII grid files (.asc) for each 480 simulation ticks or 8 hours. These ASCII outputs represent spatial flood spread and depth at a uniform grid resolution of 60 m × 60 m. To quantify flood spread (Ha) progression, first, in R-studio, all NetLogo ASCII output files were converted to raster format and projected to WGS 1984 UTM Zone 48S to ensure spatial consistency with vector boundaries and facilitate area calculations. Flood rasters were then spatially clipped to two spatial extents: (i) the entire study area polygon and (ii) the CFPP facilities area polygon, enabling separate analyses for regional and infrastructure-specific flood impacts

For each raster and time step, flooded cells were identified based on flood depths between 0.2 m and 4.0 m, representing operationally relevant inundation depths for landscape-scale flooding. The number of flooded cells within each spatial extent was counted, and flooded area was calculated by multiplying the flooded cell count by the cell area which is 0.36 ha per cell, corresponding to 60 m × 60 m cell resolution.

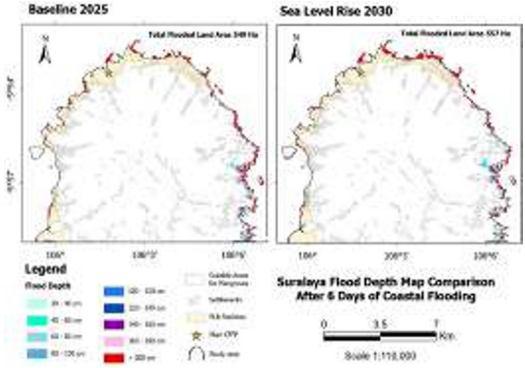

FIGURE 2. Flood depth map for baseline without mangrove 2025 and sea level rise 2030 without mangrove.

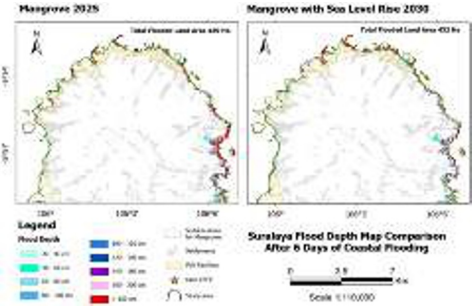

FIGURE 3. Flood depth map for baseline 2025 with mangrove and sea level rise 2030 with mangrove.

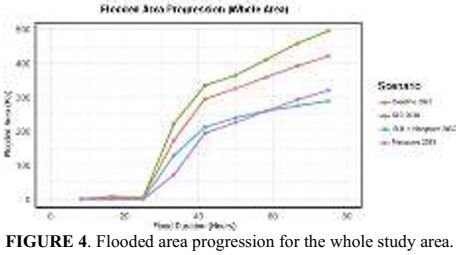

FIGURE 4. Flooded area progression for the whole study area.

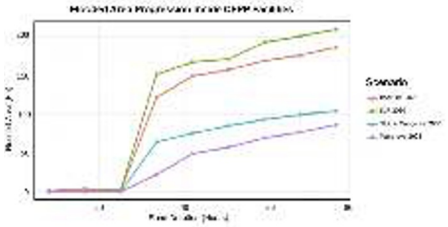

FIGURE 5. Flooded area progression within CFPP facilities area.

NetLogo simulation ticks were converted to elapsed time in hours using a constant conversion factor of 60 ticks = 1 hour, allowing direct comparison of flood progression rates across scenarios. Flooded area time series were then compiled for four scenarios: baseline conditions 2025, sea-level-rise conditions 2030, mangrove restoration 2025, and combined sea-level-rise with mangrove restoration 2030. All post-processing, area calculations, and graph plotting were performed in R using the terra, dplyr, and ggplot2 packages, with automated workflows defined in the analysis scripts. Flooded area progression curves were generated separately for the whole study area (Figure 5) and for areas within the CFPP facilities (Figure 5),

Flood progression within the CFPP facilities follows patterns consistent with the wider study area, with both mangrove scenarios exhibiting lower inundation extents than scenarios without mangroves. (Figures 3, 4, 5, and 6). Furthermore, over time, the percentage of flooded areas in the CFPP facilities area compared to the flooded area in the entire area has increased by between 25-50%. Mangrove planting has a significant impact on flood prevention in the CFPP facility area.

Based on Figures 3 and 4, mangrove restoration reduces total flooded areas after six days of coastal flooding under both present and future sea-level conditions. Under the Baseline 2025 scenario, the total flooded area decreases from 549 ha (without mangroves) to 489 ha (with mangroves), representing an absolute reduction of 60 ha or 11% decrease. Under the Sea Level Rise 2030 scenario, the flooded area declines from 557 ha (without mangroves) to 432 ha (with mangroves), corresponding to a larger absolute reduction of 125 ha or 22% decrease. This indicates that mangroves provide increasing marginal benefits under climate-intensified coastal flooding, although they are insufficient to fully offset future sea-level-rise impacts.

3.3 Floods Risk Assessment

A structured climate risk assessment is essential for evaluating the sensitivity of coastal power infrastructure to tidal flooding. This study applies to the climate risk framework from the IPCC Sixth Assessment Report, which conceptualizes risk as a function of hazard, exposure, and vulnerability. To operationalize this framework, guidance from ISO 14091 is incorporated, particularly its procedures for organizing climate risk assessments and characterizing adaptive capacity [27]. The combination of these sources provides a consistent basis for evaluating how tidal inundation affects the selected CFPP.

Following the concept of climate risk by [25], hazard refers to the potential occurrence of a climate-related physical event or trend that can cause harm. Vulnerability is the predisposition of a system to be adversely affected, determined

by its sensitivity to impact and its capacity to cope or adapt. Exposure refers to the presence of people, infrastructure, environmental assets, or economic activities in places that could be adversely affected by climate-related hazards. Briefly, the climate risk concept is defined as in Figure 6 below.

Vulnerability is quantified using depth-damage relationships adapted from [24] in Table 3, normalized between zero and two meters to reflect the sensitivity of infrastructure to increasing water depth. The depth is determined from the average flood depth in the observation area. Exposure is defined as the proportion of CFPP infrastructure located within areas that experience flooding [5]. The classification of the exposure level is based on percentage of flooded areas shown at Table 4.

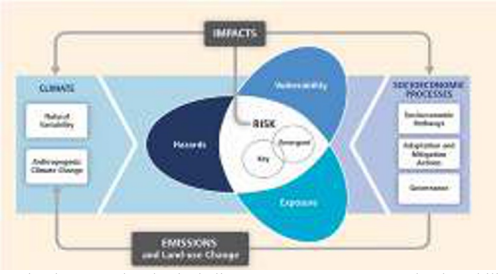

FIGURE 6. Interaction between the physical climate system, exposure, and vulnerability (IPCC, 2014)

The hazard intensity is represented by the flood derived from the flood simulation. Flood depth is classified into five levels: very low (<0.4 m), low (0.4 to 0.5 m), moderate (0.5 to 1.5 m), high (1.5 to 2 m), and very high (>2 m). This classification is the modification of flood depth parameter where flood depth of 0.2 m is dangerous to childre,n and depth above 1.5 m is dangerous to building. In this study, the flood depth for hazard assessment is calculated from the average flood depth in the observation area.

After each component is assessed, exposure and vulnerability scores are combined to form an impact level using the matrix in Table 5. This impact level is then integrated with the hazard classification following Table 6 to derive the final flood risk category. This structured approach allows flood risk to be quantified transparently and enables direct comparison across baseline and mangrove intervention scenarios.

TABLE 3. Adjusted depth-damage parameter

Water depth (m)	Damage factor	Level
0	0	Very Low
0.17	0.28	
0.3	0.48	Low
0.5	0.63	
0.7	0.72	Moderate
1	0.86	
1.3	0.91	High
1.7	0.96	
>2	1	Very High

TABLE 4. The exposure level based on percentage flooded area

Exposure Level	Percentage Area Flooded	Implications
Very Low	<5%	Minimal localized impact, high resilience (Kim et al., 2016)
Loe	5-15%	Minor service disruptions; managed via standard drainage (Sigit et al., 2023)
Moderate	15-30%	Significant community impact; potential for infrastructure "hotspots" (Andreeva et al., 2025)
High	30-50%	Widespread disruption to transport and utilities (Espada, 2014)
Very High	>50%	Critical systemic failure; high economic loss (Sigit et al., 2023)

TABLE 5. Matrix of Exposure and Vulnerability Levels (Jhong et al., 2019)

Assessment matrix for exposure and vulnerability		Level of vulnerability				
		Very high	High	Moderate	Low	Very low
Level of exposure	Very high	Severe	Severe	High	High	Moderate
	High	Severe	High	Moderate	Moderate	Low
	Moderate	High	Moderate	Moderate	Moderate	Low
	Low	High	Moderate	Moderate	Low	Very low
	Very low	Moderate	Low	Low	Very low	Very low

TABLE 6. Hazard, Exposure and Sensitivity Index Matrix (Jhong et al., 2019)

Risk Assessment Matrix		Level of exposure and vulnerability				
		Very high	High	Moderate	Low	Very low
Level of hazard	Very high	Severe	Severe	Significant	Significant	Moderate
	High	Severe	Significant	Moderate	Moderate	Minor
	Moderate	Significant	Moderate	Moderate	Moderate	Minor
	Low	Significant	Moderate	Moderate	Minor	Negligible
	Very low	Moderate	Minor	Minor	Negligible	Negligible

FIGURE 7. Area of observation for maximum inundation depth analysis.

In the observation area surrounding the main CFPP in Figure 8, the flooded area is approximately 6% of the total area for the Baseline 2025 scenario and decreased to 5% after mangrove restoration, following the Mangrove 2025 scenario. The same thing happens in the Sea Level Rise 2030 scenario, where the flooded area reaches 15% of the total area, and after mangrove restoration, Sea Level Rise 2030 + Mangrove scenario, it decreased to 11%. Thus, the exposure level for both Baseline 2025 and Sea Level Rise 2030 don't change after mangrove restoration, which is Low. The same result applies for the vulnerability level where the mangrove doesn't change the level because the average inundation depth is High for both scenarios. Using the exposure and vulnerability matrix, the overall risk level in both scenarios is Moderate.

In the Baseline 2025 scenario, the maximum flood height before and after mangrove restoration is above 200 cm and 200 cm with the Very High and High categories. In the Sea Level Rise 2030 scenario, the maximum flood height before and after mangrove restoration is above 200 cm with the Very High category. Flood heights at several points in the observation area have changed but the maximum flood height remains the same. The overall flood risk using the hazard, exposure and vulnerability matrix in the Baseline 2025 scenario has decreased from Significant to Moderate. Meanwhile, in the Sea Level Rise 2030 scenario, the flood risk either before or after mangrove restoration has not decreased and remains at the Significant risk level. Overall, mangrove restoration produces limited but

measurable reductions in flood depth and inundation extent across scenarios.

4 Discussion

The modelling results should be analyzed with regard to data quality, spatial resolution, and the foundational assumptions of the rule-based simulation. These limitations affect both the land-suitability assessment and the simulated flood progression, which helps explain the patterns observed across the different scenarios.

Estimation of carbon sequestration and vulnerability relies on generalized coefficients derived from the literature, leading to uncertainty when applied to a specific context such as the Banten CFPP. A comparison between carbon sequestration by mangroves and carbon emissions from the CFPP shows a small contribution from mangroves, accounting for only about 0.004% of the CFPP's carbon emissions. While the significance of the avoided carbon cost, estimated at approximately Rp 27.81 million per year, is relative and depends on the size and type of industry, these offsets represent a measurable and sustainable contribution of blue carbon to long-term mitigation that operates independently of plant operations.

The NetLogo model enables a relative comparison of flood behavior across scenarios but does not represent full accurate hydrodynamic processes. In this simplified flood simulation, mangroves cause measurable but scenario-dependent reductions in flood depth and inundation extent. In both the Baseline 2025 and Sea Level Rise 2030 scenarios, after six hours tidal flooding, the mangrove doesn't affect the exposure and vulnerability levels of flood risk. However, the mangrove does affect the hazard level in the Baseline 2025 scenario, but it doesn't in the Sea Level Rise 2030 scenario.

Simulation results demonstrate that mangrove restoration can reduce flooded areas by up to 22%, although this effect remains spatially limited and scenario-dependent. This finding indicates that the primary function of mangroves in this context is to delay and partially mitigate the impact of flooding, rather than prevent inundation entirely. Given the relatively small area of mangroves compared to the study area, the flood mitigation and delay effects are spatially limited and primarily occur in the area surrounding the mangroves and are highly dependent on the magnitude of water level rise.

Flood mitigation in the model arises mainly from the elevation-based representation of mangroves, rather than from explicit modeling of vegetation roughness or wave energy dissipation. In this model, mangrove areas are represented as topographic modifications that affect water retention and flow paths. Thus, the resulting flood risk reduction reflects the buffering function of topography and does not fully represent the complexity of real-world hydrodynamic processes occurring in mangrove ecosystems. While this approach is adequate for conceptual assessment, future research should incorporate dynamic vegetation characteristics through manning's number, and other hydrological forces such as precipitation, river discharge, and water infiltration, to more realistically represent the interactions between mangrove ecosystems and flood dynamics.

Despite these model simplifications, the framework acts as a guide for decision-makers to improve the effectiveness of integrated climate-risk strategies. Since mangrove-based carbon sequestration is relatively modest and makes up only a small part of industrial output, the findings suggest that blue carbon should be considered a complementary asset. To meet decarbonization targets, industries could combine mangrove restoration with technical solutions, such as CCS, within power plant infrastructure. Similarly, to improve infrastructure resilience against rising sea levels, mangroves should be combined with engineered protections, such as reinforced sea walls or elevated embankments. This hybrid approach, mixing nature-based and engineered solutions, provides a stronger defense than either method could offer alone.

To make the framework more practical, future research should look into socio-economic feasibility, governance issues, and land-use competition. All of these factors significantly affect the success of mangrove restoration in industrial areas. Including institutional capacity and stakeholder dynamics would enable a better assessment of the long-term viability of mangrove-based interventions. By connecting biophysical modeling with these various factors, the framework can more effectively support government and industry in creating sustainable, long-term resilience strategies for Indonesia's coastal energy sector.

5 Conclusion

This research presents a cohesive conceptual framework for assessing the dual role of blue carbon ecosystems, particularly mangroves, in climate mitigation and the reduction of coastal flood risk for CFPPs. The first part finds suitable areas for mangrove restoration, the amount of carbon sequestration, and the offset from carbon taxes. The

second part uses a rule-based coastal flood model and a climate-risk assessment to see how restoring mangroves affects the depth, exposure, and spread of flooding.

When applied to a typical CFPP in Banten Province, the framework shows that the suitable area for mangrove restoration is relatively small compared to the whole study area. This small restoration area results in low carbon sequestration and limited avoidance of carbon credit. These offsets, while small, represent a measurable and sustainable contribution of blue carbon to long-term mitigation that operates independently of plant operations.

Restoring mangroves can lower the depth of flooding and the area that is flooded, but only to a small extent, and the effects vary depending on the situation. Mangrove restoration gives bigger impact to the overall flood-risk in Baseline than Sea Level Rise scenario where the mangrove can lower flood risk from Significant to Moderate through the reduction of the maximum flood depth. The flood simulation also shows that the mangrove spatial configuration plays important roles in the exposure and vulnerability level of flood risk. From a risk mitigation perspective, the framework serves as a strategic roadmap for a hybrid protection model. Since mangroves alone cannot completely offset industrial emissions or provide full flood protection, they need to be part of a layered defense approach. For reducing carbon emissions, the small storage of blue carbon should be supported by carbon capture technologies such as CCS. For physical resilience, mangroves should serve as a "first line of defense" alongside engineered structures.

The framework is designed as a practical decision-support tool rather than an accurate predictive engineering model. Its value lies in its ability to combine ecological suitability, carbon valuation, and flood dynamics into a single analytical framework that allows government and industry to identify where nature-based solutions reach their physical limits. Future endeavors should broaden the framework to include socio-economic viability, governance structures, and dynamic ecological processes, including sediment accretion and mangrove adaptation in response to rising sea levels. Strengthening these parts will make the framework more useful for long-term planning and decision making in Indonesia's coastal power sector.

Overall, this study lays the groundwork for combining blue carbon ecosystems with coastal infrastructure resilience. It also supports the idea that nature-based solutions should be used alongside, rather than stand alone solution for Indonesia's plans to adapt to climate change and transition to cleaner energy sources.

6 References

1. D. M. Alongi, Carbon Manage. 3(3), 313–322 (2012).
2. M. F. Adame, J. Kelleway, K. W. Krauss, C. E. Lovelock, and J. B. Adams, BioScience 74(4), 253–268 (2024).
3. N. Andreeva and N. Nikolova, “Assessment of coastal receptors' exposure vulnerability to flood hazard along Varna regional coast,” in International Conference on Coastal Engineering (Varna, 2025).
4. V. B. Arifanti, J. B. Kaufmann, Subarno, M. Ilham, A. Tosiani, and N. Novita, Glob. Change Biol. 0(0), 1-16 (2022).
5. A. Assab, J. Clim. Finance 11, 100066 (2025).
6. Badan Perencanaan Pembangunan Daerah, Peta Rencana Pola Ruang Wilayah Kota Cilegon Tahun 2010-2030 (Pemerintah Kota Cilegon, Cilegon, 2011).
7. Badan Informasi Geospasial (BIG), Digital Elevation Model Nasional (DEMNAS), v1.0 (BIG, Jakarta, 2018).
8. Badan Penanggulangan Bencana Daerah Kota Cilegon, Kajian Risiko Bencana (KRB) Kota Cilegon Tahun 2023–2027 (Pemerintah Kota Cilegon, Cilegon, 2023).
9. BankTrack, “Perusahaan Listrik Negara (PLN)” (2025), available at https://www.banktrack.org/company/pt_pln.
10. B. Choudhary, V. Dhar, and A. S. Pawase, J. Sea Res. 199, 102504 (2024).
11. S. Coles, An Introduction to Statistical Modeling of Extreme Values (Springer, London, 2001).
12. Copernicus Climate Change Service (C3S), ERA5: Fifth generation of ECMWF atmospheric reanalyses of the global climate (Copernicus Climate Data Store, 2017).
13. Global Energy Observatory, “Coal Power Plants in Indonesia” (2025), available at https://database.earth/energy/power-plants/coal-power/indonesia.
14. N. C. Duke, “Mangrove floristics and biogeography,” in Tropical Mangrove Ecosystems, edited by A. I. Robertson and D. M. Alongi (American Geophysical Union, Washington DC, 1992), pp. 63–100.
15. C. Earlie, G. Masselink, and P. Russell, Earth Surf. Process. Landf. 43(6), 1213–1228 (2018).
16. ESA Climate Office, Climate Hazards Group InfraRed Precipitation with Station data (CHIRPS) version 2.0 (European Space Agency, 2022).
17. R. J. Espada Jr., “Spatial analysis and modelling of flood risk and climate adaptation capacity of urban

communities and critical infrastructures," Ph.D. thesis, University of Southern Queensland, 2014.
18. A. H. Fattah, Suntoyo, H. A. Damerianne, and Wahyudi, IOP Conf. Ser.: Earth Environ. Sci. 135(1), 012024 (2018).
19. Government of the Republic of Indonesia, Presidential Regulation No. 98 of 2021 on Carbon Economic Value (Jakarta, 2021).
20. L. Hawker, P. Uhe, L. Paulo, J. Sosa, J. Savage, C. Sampson, and J. Neal, Environ. Res. Lett. 17(2), 024016 (2022).
21. T. Hengl, J. M. de Jesus, G. B. M. Heuvelink, M. R. Gonzalez, M. Kilibarda, A. Blagotić, W. Shangguan, M. N. Wright, X. Geng, and B. Bauer-Marschallinger, PLOS ONE 12(2), e0169748 (2017).
22. G. J. Huffman, D. T. Bolvin, D. Braithwaite, K. Hsu, R. J. Joyce, C. Kidd, E. J. Nelkin, and P. Xie, Integrated Multi-satellite Retrievals for GPM (IMERG) – Final run, version 6 (NASA Goddard Space Flight Center, 2020).
23. J. Huizinga, H. De Moel, and W. Szewczyk, Global flood depth-damage functions: Methodology and the database with guidelines (JRC European Commission, 2017).
24. IPCC, Managing the Risks of Extreme Events and Disasters to Advance Climate Change Adaptation, edited by C. B. Field et al. (Cambridge University Press, Cambridge, 2012) .
25. ISO, ISO 14091: Adaptation to climate change — Guidelines on vulnerability, impacts and risk assessment (International Organization for Standardization, Geneva, 2021).
26. B.-C. Jhong, J. Huang, and C.-P. Tung, Water Resour. Manage. 33(10), 3377–3400 (2019).
27. H. Kim, D.-K. Lee, and S. Sung, Sustainability 8(2), 134 (2016).
28. R. C. Leong, D. A. Friess, B. Crase, W. K. Lee, and E. L. Webb, Estuar. Coast. Shelf Sci. 202, 185–192 (2018).
29. D. Murdiyarso, M. N. J. Matthews, P. B. P. S. K. P. Sasmito, and D. A. F. G. Gumert, Nat. Clim. Chang. 5(12), 1089–1092 (2015).
30. Ministry of Marine Affairs and Fisheries, Regulation No. 1 of 2025 on Implementation of Carbon Economic Value in the Marine Sector (Jakarta, 2025).
31. H. A.-E. Monsef, A. S. H. Aguib, and S. E. Smith, J. Afr. Earth Sci. 83, 1–9 (2013).
32. I. Pal, A. Kumar, and A. Mukhopadhyay, Annu. Rev. Environ. Resour. 48(1), 681–712 (2023).
33. PT PLN (Persero), Rencana Usaha Penyediaan Tenaga Listrik (RUPTL) 2025-2034 (PLN, Jakarta, 2025).
34. M. Pronk, A. Hooijer, D. Eilander, A. Haag, T. De Jong, M. Vousdoukas, R. Vernimmen, H. Ledoux, and M. Eleveld, Sci. Data 11(1) (2024).
35. Y. E. Saputriningrum and D. Mardiatno, J. Bumi Indones. 7(3) (2018).
36. M. Shokatian-Beiragh, M. Banan-Dallalian, A. Golshani, M. N. Allahdadi, and M. Samiee-Zenoozian, Reg. Stud. Mar. Sci. 77, 103630 (2024).
37. A. Sigit, M. Koyama, and M. Harada, Sustainability 15(24), 16856 (2023)
38. B. Suprakto, Soemarno, Marsoedi, and D. Arfiati, Int. J. Ecosystem 4(3), 115-121 (2014).
39. L. N. Syahid, A. D. Sakti, R. Virtriana, K. Wikantika, W. Windupranata, S. Tsuyuki, R. E. Caraka, and R. Pribadi, Remote Sens. 12(22), 3734 (2020).
40. B. Tozer, D. T. Sandwell, W. H. F. Smith, C. Olson, J. Beale, and P. Wessel, Earth Space Sci. 6(10), 1847–1864 (2019).
41. T. Wijayanto, D. F. Hakam, and P. N. Kemala, Sustainable Futures 9, 100344 (2025).
42. D. Xie, C. Schwarz, M. G. Kleinhans, Z. Zhou, and B. van Maanen, J. Geophys. Res.: Earth Surf. 127(3) (2022).